Supporting Information

Advanced H_2-Storage System Fabricated via Chemical Layer Deposition in a Well-Designed Porous Material Template

Yanhui Guo[a], Minghong Wang[b], Guanglin Xia[a], Xiaohua Ma[a,c], Fang Fang[a], Yonghui Deng*[b]*

[a] Department of Materials Science, Fudan University, Shanghai, 200433 China

[b] Department of Chemistry, State key Laboratory of Molecular Engineering of Polymers, Fudan University, Shanghai, 200433 China

[c] Center of Special Materials and Technology, Fudan University, Shanghai, 200433 China

Correspondence and requests for materials should be addressed to F. Fang, and Y. H. Deng.
email: f_fang@fudan.edu.cn, yhdeng@fudan.edu.cn.

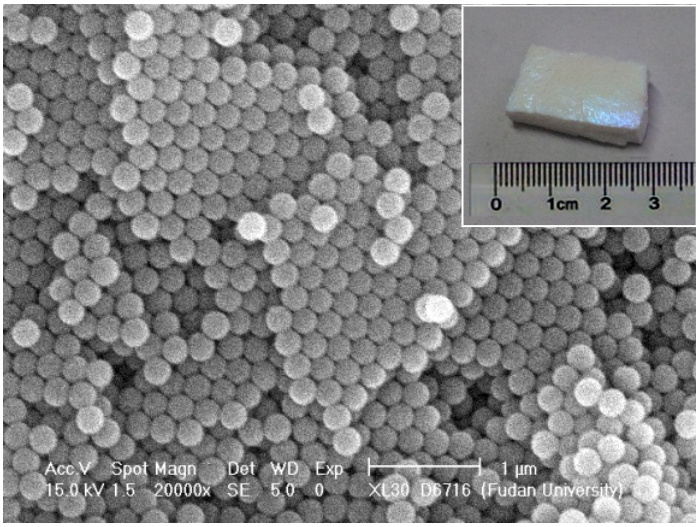

Figure S1 SEM image of colloidal crystals consisting of uniform silica spheres of 250 nm. The inset shows the photograph of a piece of colloidal silica crystals

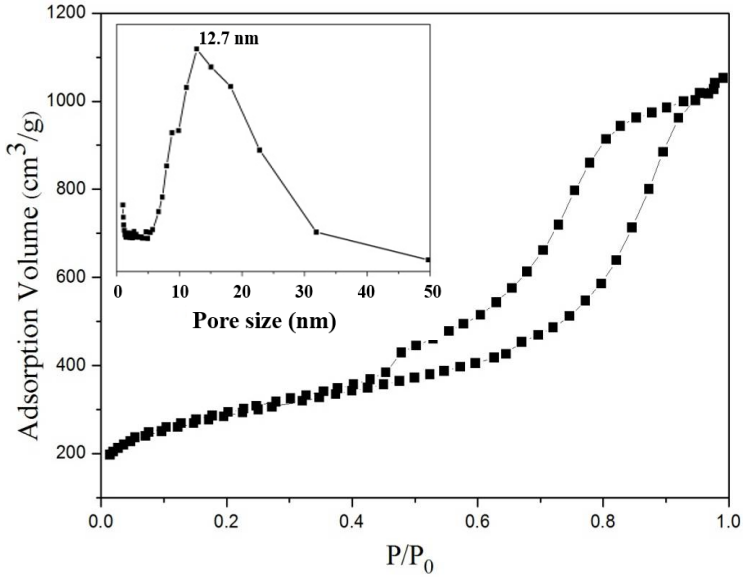

Figure S2 N_2 sorption isotherms and pore size distributions of the hierarchically macro-mesoporous carbon with macropore of 250 nm and mesopore of 12.7 nm.

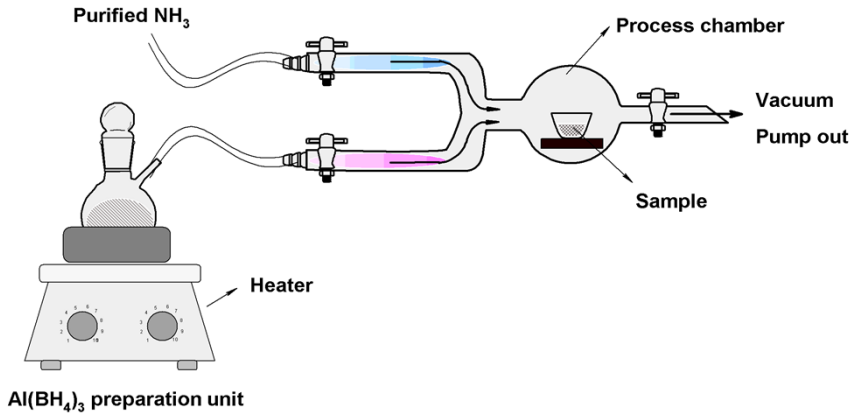

Figure S3. Schematic representation of the procedure for the deposition of ammine aluminum borohydrides (AAB) in ce-confined into carbon scaffolds via the CLD methodology.

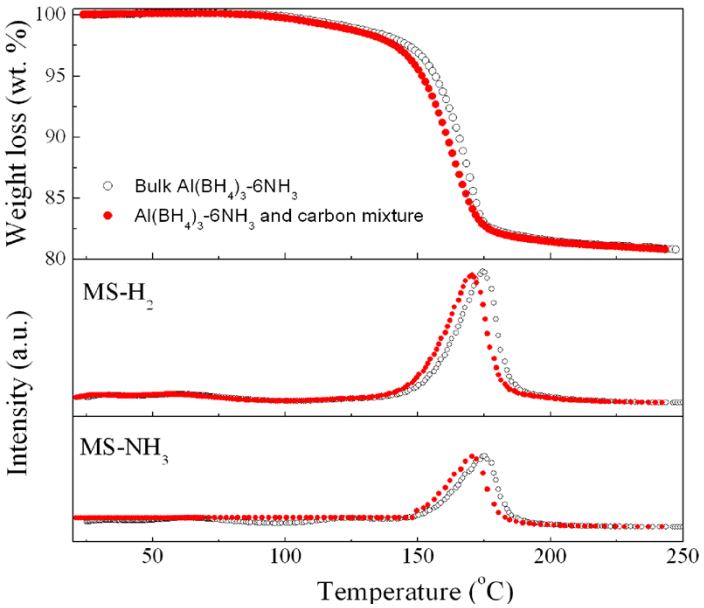

Figure S4 TGA-MS spectra of the pure $Al(BH_4)_3(NH_3)_6$ (in black line) and the physical mixture of $Al(BH_4)_3(NH_3)_6$ with HOPC (in red line).

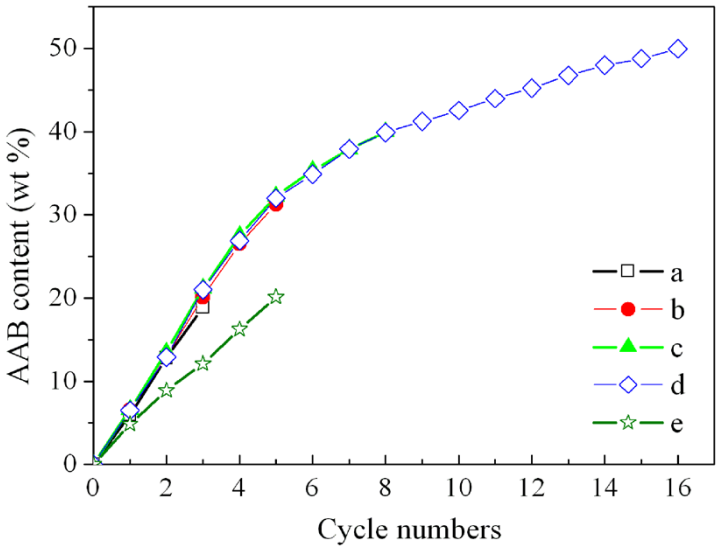

Figure S5. The increment of uploading capacity with the proceeding of reaction cycles for various carbon templates under different conditions; a: C-20; b: C-30; c: C-40 d: C-50 with the time of 2 h for ammonia physisorption and then the time of 0.5 h for vacuuming to remove residual ammonia during the first cycle; e: C-20; with the absorption time of ammonia for 2 h and then the time of 0.8 h for vacuuming to remove residual ammonia during the first cycle.

It clearly indicates that, with the proceeding of reaction cycles, the kinetics of the increment of loading capacity decreases, which can be attributed to the fact that upon the uploading of ammine aluminum borohydrides, the entrance become fewer and smaller, which hinders the transmission of precursors into the pore. Moreover, via adjusting the capacity of NH_3 adsorbed inside the templates during the first cycle, i.e., increasing the time of removing NH_3 from 0.5 h to 0.8 h, the weight gain for every cycle decreased for the same carbon scaffolds with a diameter of 250 nm. Therefore, the morphology and capacity of the uploaded $Al(BH_4)_3(NH_3)_6$ can be readily tuned by adjusting the capacity of NH_3 adsorbed during the 1st cycle.

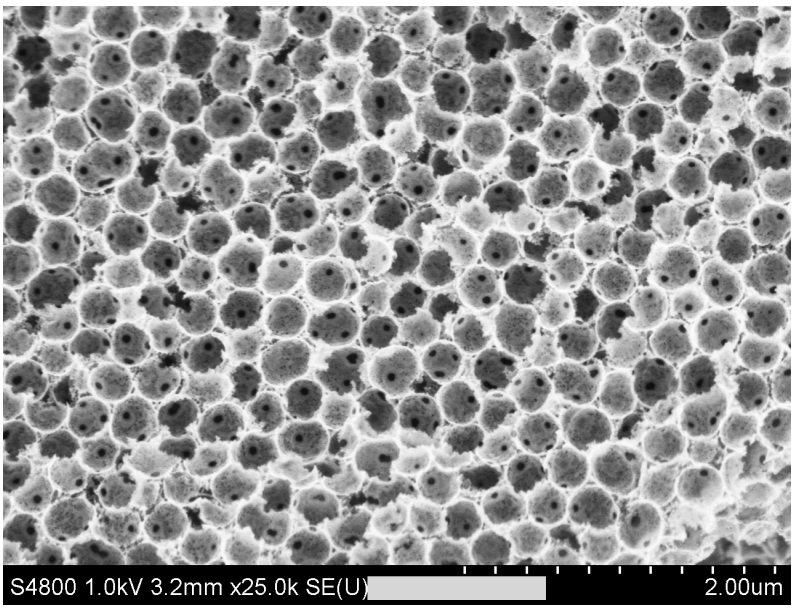

Figure S6 SEM image of C-30

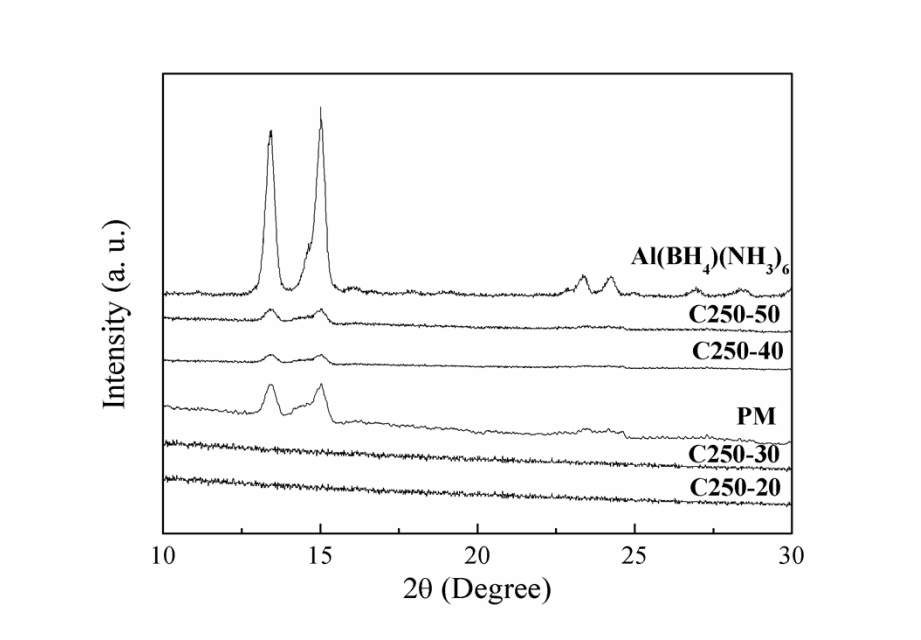

Figure S7. XRD patterns of a physical mixture of 30 wt.% $Al(BH_4)_3(NH_3)_6$ with carbon (PM), and $Al(BH_4)_3(NH_3)_6$ confined into carbon scaffold with various weight capacity, including bulk $Al(BH_4)_3(NH_3)_6$ for reference.

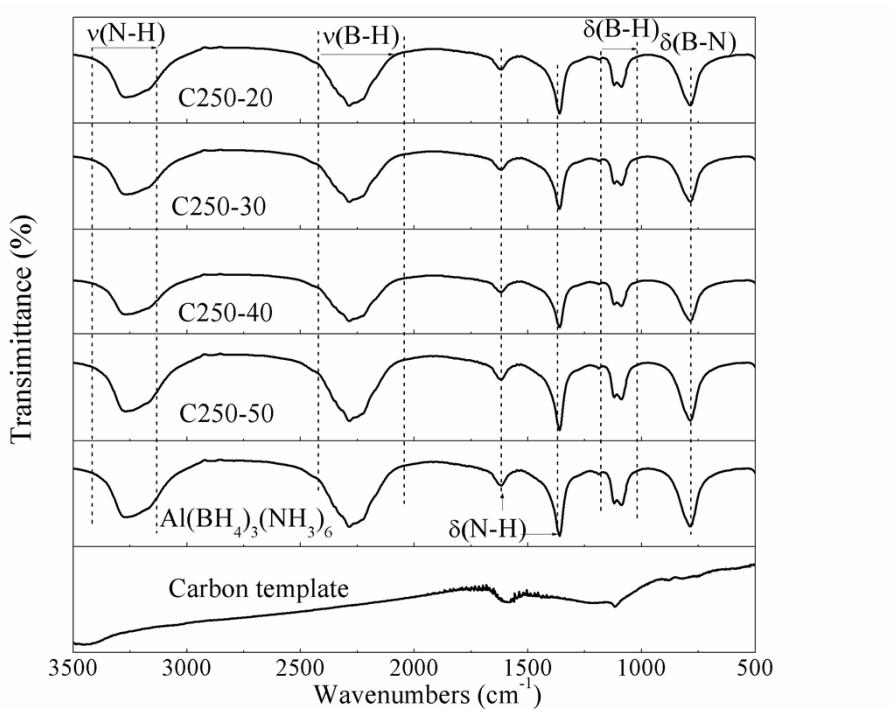

Figure S8. FT-IR spectra of $Al(BH_4)_3(NH_3)_6$ confined into carbon scaffold with various weight capacity via CLD, including bulk $Al(BH_4)_3(NH_3)_6$ and carbon templates for reference.

The presence of similar absorption peaks for N-H and B-H bonds of nanoconfined $Al(BH_4)_3(NH_3)_6$ with bulk $Al(BH_4)_3(NH_3)_6$ provides the further evidences for the formation of BH_4 and NH_3 moieties of $Al(BH_4)_3(NH_3)_6$ inside the pores of carbon templates. Moreover, the B-N bonds at around 780 cm^{-1} indicates the interaction of BH_4 with NH_3 groups within $Al(BH_4)_3(NH_3)_6$, in which the combination of B-H and N-H bonds mainly affords its H_2 release.

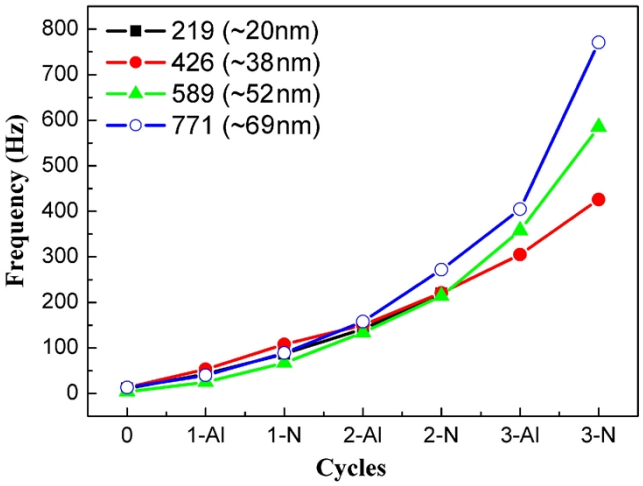

Figure S9 Deposition of HAAB with various thichness on QC substrate.

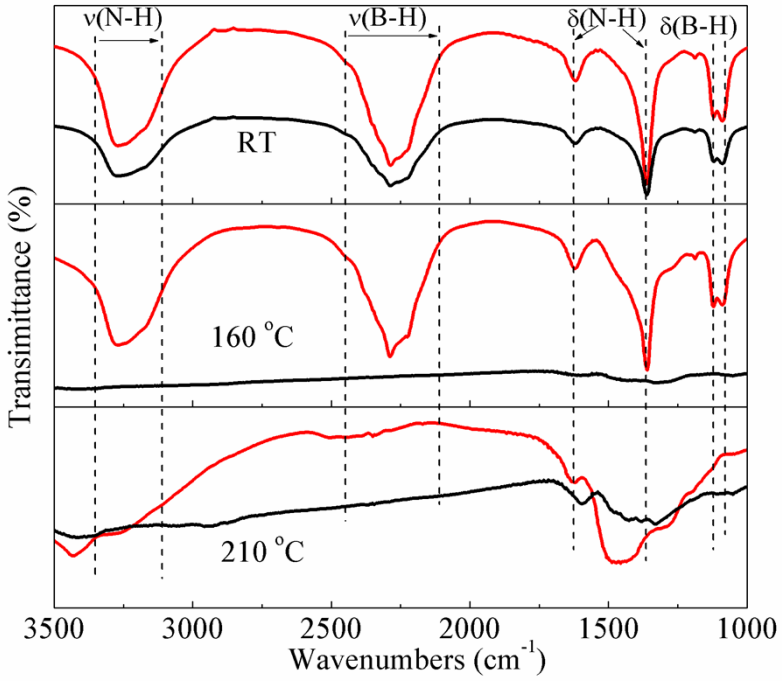

Figure S10. FTIR spectra for bulk (in red line) and nanoconfined (in black line) $Al(BH_4)_3(NH_3)_6$ at room temperature (RT) and its products after heating to 160 °C and 210 °C, respectively. The heating rate is 5 °C/min.

The spectra of bulk and nanoconfined $Al(BH_4)_3(NH_3)_6$ show the characteristic peaks of B-H and N-H bonds. Upon heating, the combination of $H^{\delta-}$ of BH_4 with $H^{\delta+}$ of NH_3 mainly accounts for the H_2 desorption from ammine metallic borohydrides. Therefore, after heating to 160 °C, B-H and N-H bonds disappeared for the nanoconfined $Al(BH_4)_3(NH_3)_6$, indicating the participation of BH_4 groups and NH_3 groups in the process towards H_2 release, which amounts to over 95% of its total releasable H_2 capacity as evinced from TG and TPD results. In contrast, for the bulk $Al(BH_4)_3(NH_3)_6$ heated to 160 °C, there are clear peaks attributed to the B-H and N-H bonds, suggesting only partial decomposition for a small amount of H_2 and NH_3 release, which accords well to the TG and TPD results. Upon further elevating the heating temperature to 210 °C, all the absorption bands of bulk $Al(BH_4)_3(NH_3)_6$ assigned to the NH_3 group and the BH_4^{-1} ion disappeared, due to the combination of N-H bonds and B-H bonds for H_2 desorption. These results indicate the significantly improved H_2 release kinetics at relatively lower temperature of $Al(BH_4)_3(NH_3)_6$ space-confined into carbon scaffolds via the CLD methodology.

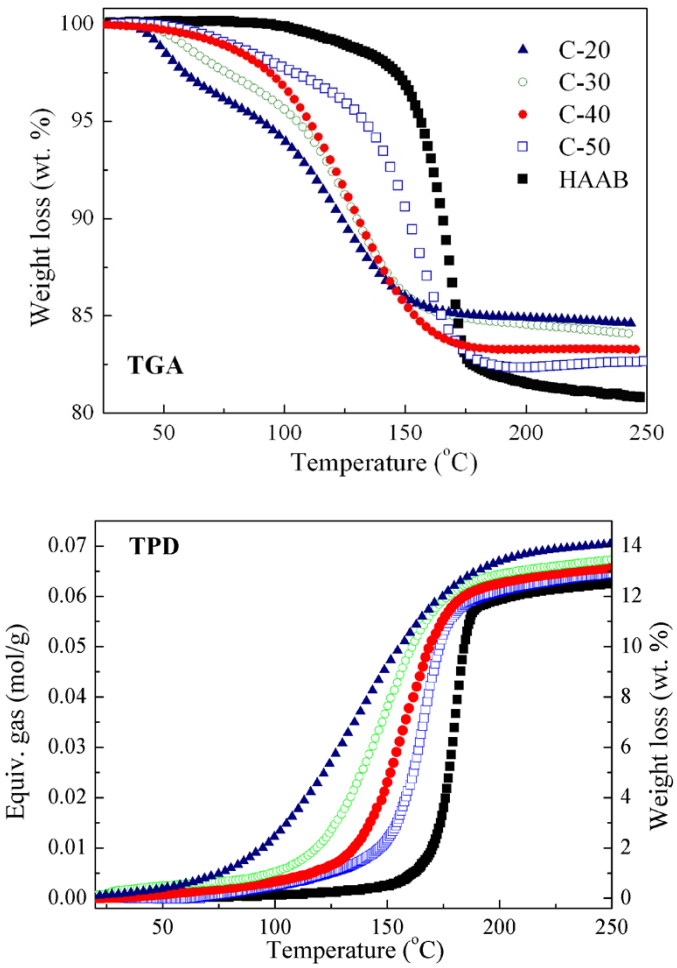

Figure S11. TGA and TPD profiles of $Al(BH_4)_3(NH_3)_6$ confined into scaffolds upon heating to 250 °C using a heating rate of 5 °C/min, including bulk $Al(BH_4)_3(NH_3)_6$ (HAAB) for comparison.

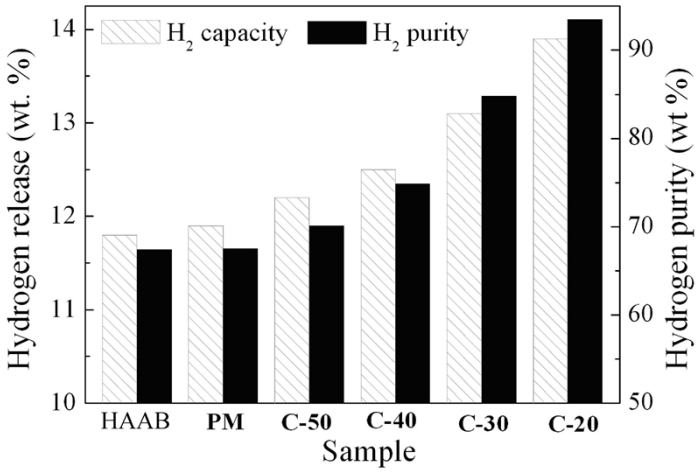

Figure S12 Histogram of capacity and purity of hydrogen evolution from HAAB, physical mixture of HAAB and carbon scaffold (PM), and HAAB@HOPC (C-20, C-30, C-40, C-50) by 250 ^{o}C.

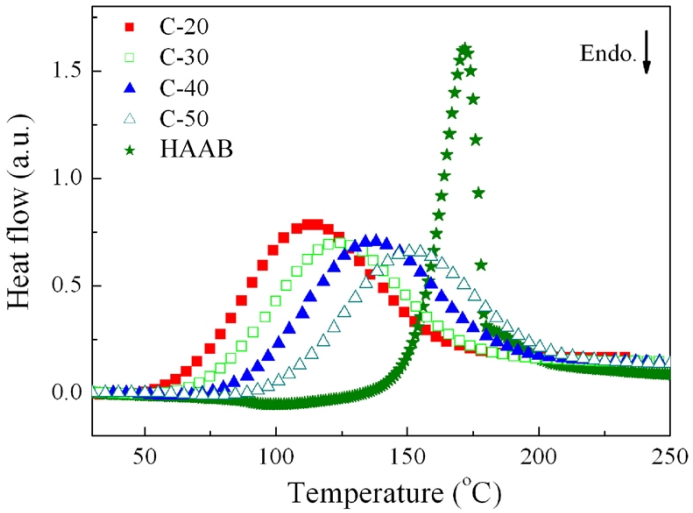

Figure S13. DSC profiles of HAAB and HAAB@HOPC (C-20, C-30, C-40, C-50) upon heating to 250 °C using a heating rate of 5 °C/min.

The as-prepared $Al(BH_4)_3(NH_3)_6$ exhibits a single exothermic peak at 172 °C with a shoulder, corresponding to an enthalpy of approximately -6.75 KJ/mol H_2. Comparable traces upon hydrogen liberation were observed for $Al(BH_4)_3(NH_3)_6$ nanoconfined into scaffolds at relatively lower temperature, with one exothermic signal significantly broadened in comparison with bulk reagent in good accordance with the MS results. However, the integration of the endothermic peaks (Table S1) indicates that the total enthalpy of the reaction increases slowly with the decreasing capacity of $Al(BH_4)_3(NH_3)_6$ inside the carbon matrix, which is consist with the diminution of ammonia released upon dehydrogenation due to the fact that ammonia release is significantly endothermic from borohydrides. The similar phenomenon was also found for the hydrogen release process of ammonia borane (AB) infiltrated into the mesopores of SBA-15. It suggests that different solid products formed for $Al(BH_4)_3(NH_3)_6$ inside the carbon scaffolds derived from more ammonia participates in hydrogen release compared with the pure one resulting in the more exothermicity for dehydrogenation. Moreover, compared to decomposition of the other typical hydrogen storage materials based on HB-NH combination, e.g., neat AB (-21 KJ/mol H_2), the significantly less exothermic characterization of nanoconfined $Al(BH_4)_3(NH_3)_6$ provides a great potential for its reversible hydrogen storage with proper chemical modification. Therefore, the tremendous enhancement of hydrogen desorption performance at low temperature not only relates to the improved dehydrogenation kinetics but also the more favorable thermodynamics to some extent, compared to bulk counterparts, due to the reduction of particle sizes induced by the nanoconfinement procedure.

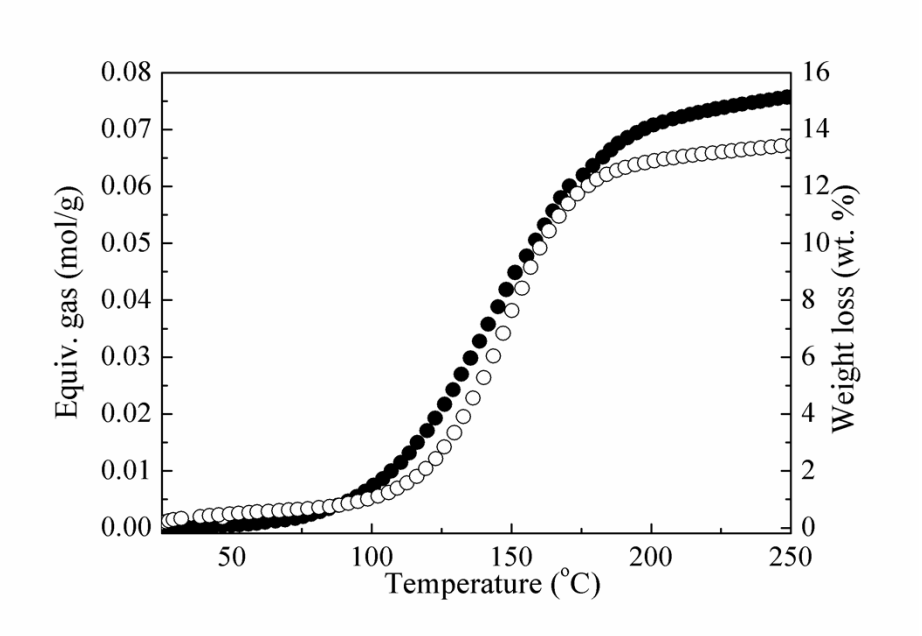

Figure S14. TPD results of C-30 and $Al(BH_4)_3(NH_3)_5$@HOPC (●) upon heating to 250 °C using a heating rate of 5 °C/min.

Table S1. The peak temperature and Enthalpy data for hydrogen release from $Al(BH_4)_3(NH_3)_6$ loaded in carbon scaffolds, the data of bulk $Al(BH_4)_3(NH_3)_6$ were also listed for comparison.

Sample	Peak Temperature (^oC)	Enthalpy (KJ/mol H_2)
C-20	112.5	-7.23
C-30	122.9	-6.81
C-40	135.8	-6.79
C-50	150.8	-6.78
$Al(BH_4)_3(NH_3)_6$	172.1	-6.75